

Full Length Article

Nanobubbles in graphene-based nanofluids: Unraveling the mechanisms behind nucleation, behaviour and thermophysical properties using a molecular approach

Hamidreza Hassanloo^{*}, Xinyan Wang

Centre for Advanced Powertrain and Fuels, Brunel University London, Uxbridge UB8 3PH, United Kingdom



ARTICLE INFO

Keywords:

Graphene nanofluids
Molecular dynamics simulation
Nanobubbles nucleation
Thermophysical properties

ABSTRACT

Significant endeavors have been undertaken to substitute conventional thermal fluids with those possessing enhanced thermophysical properties, wherein nanoscale phenomena, particularly the integration of nanoparticles like graphene, play a crucial role. Graphene's exceptional properties and interactions with surrounding molecules make it an ideal candidate for nanoparticle integration, particularly in renewable energy applications such as solar energy. The introduction of dissolved gases, especially in industrial processes like electrochemical reactions, further influences fluid behavior and thermophysical properties, potentially leading to the formation of nanobubbles, with this alteration becoming even more pronounced. This study employs molecular dynamics simulations to investigate nanobubble formation, behavior, and their impact on the inherent properties of graphene-water and graphene-methanol nanofluids, featuring a $9.5 \text{ nm} \times 9.5 \text{ nm}$ graphene sheet immersed in 98,000 water molecules and 48,000 methanol molecules, respectively. The findings reveal distinct behaviors depending on the host liquid, with two-atom gases forming graphene-nanobubbles in water-based nanofluid, while nitrogen and hydrogen predominantly form bulk nanobubbles in methanol. Moreover, the presence of formed nanobubbles and dispersed graphene increases water viscosity but decreases it in two-atom gas/graphene-methanol nanofluids. The lowest viscosity is recorded for the graphene/methanol sample with hydrogen nanobubbles at 0.00053 Pa.s, while the highest viscosity is observed for the oxygen methanol sample without nanobubbles at 0.00068 Pa.s. Conversely, the specific heat capacity of water-based nanofluids decreases due to nanobubbles and dispersed graphene, particularly pronounced in oxygen/graphene-nanofluid. While in methanol-based nanofluids, the specific heat capacity increases, notably in oxygen-graphene/methanol nanofluids.

1. Introduction

The urgent need to combat carbon emissions necessitate prioritizing renewable energy production and addressing excessive energy consumption through efficient energy utilization. This requires the integration of effective thermal management and transfer technology across the entire product design and consumption process [1,2]. Such thermal management and transfer technologies find applications in various sectors, ranging from everyday electronic devices to large-scale equipment in various industries. For instance, in solar thermal collectors that harness solar energy, heat pipe technology is employed to absorb and transfer the solar energy to a secondary heat transfer fluid. An important consideration in thermal management and transfer technology is the

careful choice of working fluids. Extensive research has focused on developing fluids with improved intrinsic characteristics. Notably, the emergence of nanofluids (NFs), which are combinations of traditional coolants such as water or alcohol and conductive solid particles, have brought significant advancements [3–8].

The ground-breaking discovery of graphene (G), a two-dimensional material composed of a single layer of carbon atoms arranged in a hexagonal lattice which possesses exceptional properties, including high mechanical strength, thermal conductivity, specific surface area, carrier mobility, and chemical stability at room temperature pave the way of innovative solutions in numerous industries [8–14]. The unique electronic structure and inherent 2D nature of G contribute to its remarkable sensitivity to the surrounding environment. With its high surface-to-volume ratio, graphene has emerged as a versatile sensing material for

^{*} Corresponding author.

E-mail address: Hamidreza.Hassanloo@brunel.ac.uk (H. Hassanloo).

<https://doi.org/10.1016/j.fuel.2024.132517>

Received 12 March 2024; Received in revised form 4 June 2024; Accepted 12 July 2024

Available online 19 July 2024

0016-2361/© 2024 The Author(s). Published by Elsevier Ltd. This is an open access article under the CC BY license (<http://creativecommons.org/licenses/by/4.0/>).

Nomenclature

NB	Nanobubble
NF	Nanofluid
G	Graphene
GNB	Graphene nanobubble
ns	Nanosecond
wt %	Weight fraction

NBs can be broadly categorized into two types: bulk NBs and surface NBs. Bulk NBs refer to spherical gas-filled bubbles with a diameter smaller than 1 μm . On the other hand, surface NBs are gas-filled pockets found on a surface, typically taking the shape of a spherical cap. The height of surface NBs generally falls within the range of 10 nm to 100 nm, while the radius of the contact line typically ranges from 50 nm to 500 nm [19,20]. Graphene nanobubbles (GNBs) have garnered significant interest for their ability to trap gas volumes and their potential applications in nanoscale engineering. However, the conventional methods for fabricating graphene nanobubbles are complex and require specialized equipment, such as subjecting graphite samples to high temperatures or pressures. These methods can vary depending on the desired gas trapped within the NB [18,21]. Interestingly, the weak interlayer attraction in graphite allows individual layers of G to be extracted for various purposes. For instance, An et al. [18] demonstrated the production of GNBs through water splitting. By applying a large potential difference, they observed the splitting of water molecules into hydrogen and oxygen. The trapped NBs in G were then identified using phase imaging in tapping mode AFM. The hydrogen captured by the GNBs exceeded the theoretical binding capacity, showing promise for achieving hydrogen storage targets set by the United States Department of Energy.

Extensive endeavors have been dedicated to the comprehensive characterization of NBs in the liquid phase, employing a combination of experimental techniques and numerical simulations [22–26]. These efforts aim to gain a deeper understanding of NBs, their properties, and their behavior within the liquid medium. Li et al. [27] conducted an investigation on the formation and coalescence of NBs under specific conditions. Their study involved using G as a solid substrate, which remained fixed in its initial position throughout the simulations. A layer of liquid water was placed on top of the graphene substrate, with gas molecules randomly distributed within the liquid water. The liquid water was represented using the Simple Point Charge (SPC) model. The results revealed that as the gas concentration increased, a greater number of stable bulk NBs were observed. Furthermore, the distance between surface NBs and the strength of solid–gas interactions played a significant role in the formation of a gas-enrichment layer at the solid–liquid interface. In an atomic-level study, Iakovlev et al. [28] investigated argon GNBs. They employed argon atoms as trapped substances within a curved G sheet, creating a unique two-dimensional crystal structure. Another G sheet was frozen perpendicular to the substrate, enhancing the stability of the NB. They observed in contrast to nanotubes, which have limited capacity to accommodate only a few dozen atoms, these heterostructured NBs exhibited the remarkable ability to

accumulate millions of atoms and molecules which can be considered as a thermodynamic system. Dockar et al. [29] conducted a study to investigate the mechanical stability of surface nanobubbles under negative pressure, revealing a fascinating departure from the behavior predicted by the Blake threshold in experimental studies. In their research, they employed molecular dynamics simulations with fluid and gas atoms confined between upper and lower solid walls. Their findings revealed a cavitation threshold for small bubble cavitation that was considerably lower than the conventional Blake threshold prediction. In a molecular dynamics simulation conducted by Mi et al. [30], the impact of seawater salinity, pressure, and temperature on CH_4 hydration formation was investigated in both the montmorillonite nanopore and the surrounding bulk solution. The study revealed that elevated temperatures facilitate the aggregation of CH_4 molecules, resulting in the formation of NBs, while simultaneously impeding hydrate formation. Specifically, under high temperature conditions, the NB within the nanopore exhibited a gradual decomposition, while an exceptionally large cylindrical NB grew in the bulk solution outside the nanopore. Hong et al. [31] conducted molecular dynamics simulations to model aqueous solutions containing NBs with varying porosities. To investigate the effects of porosity and temperature on transport properties, they removed water molecules within a specific radius at the center of the simulation box. The results showed that the viscosity of the nanobubble aqueous solution significantly decreased with increasing porosity. On the other hand, the diffusivity of the nanobubble solutions considerably increased with increasing temperature. However, the relationship between self-diffusion coefficients and porosity deviated from the expected trend predicted by the Stokes-Einstein equation, possibly due to the presence of hard hydrogen bonds formed at the liquid–air interface of the NBs.

While previous studies have contributed significantly to our understanding of NBs, they have predominantly focused on investigating the interaction of NBs with only solid particles [32], often with fixed solid particles, or within pure liquid environments without any NPs [33]. However, in real-world industrial applications, dispersed solid particles freely interact with their surroundings, particularly with host liquids, triggering nanoscale mechanisms that alter the thermophysical properties of host mediums essential for their applications. Notably, the creation of nanolayers around particles influences a crucial property, playing a pivotal role in fluid flow and heat transfer behavior, impacting parameters like the Reynolds number, pressure loss, and Nusselt number [34]. Moreover, nanoscale mechanisms induced by adding NPs enhance properties crucial for energy applications, particularly viscosity. A substantial average viscosity enhancement of 47.12 % was noted at a 0.15 % volume concentration of G at 50 °C in water-based NFs for heat transfer applications [35]. Additionally, G-based NFs exhibit considerably higher thermal conductivity compared to metal oxide NFs, even at lower concentrations [36]. These NFs, including G-methanol NFs, exhibit properties crucial for energy applications, particularly as working fluids in solar energy systems [37]. Furthermore, previous studies have primarily utilized pre-defined NBs, neglecting a comprehensive exploration of NB behavior from the nucleation step in NFs. Moreover, these studies have predominantly emphasized fundamental aspects, like structure parameters of nanobubbles, or limited engineering applications, lacking a comprehensive examination of NBs from multiple perspectives to provide a clear understanding of their behavior and diverse applications in industrial settings. This study aims to bridge these gaps by comprehensively investigating the behavior and applications of NBs in industrial applications. The possibility of NB formation through the dissolution of gases, namely oxygen (O_2), hydrogen (H_2), nitrogen (N_2), and carbon dioxide (CO_2), in two potential G-based NFs, namely water and methanol-based fluids, is examined. Furthermore, the behavior and thermophysical properties of NFs were investigated using molecular dynamics simulation to integrate both fundamental aspects and engineering applications of such complex fluids, with the aim of gaining a deeper understanding of the role of NBs in complex fluids in the presence

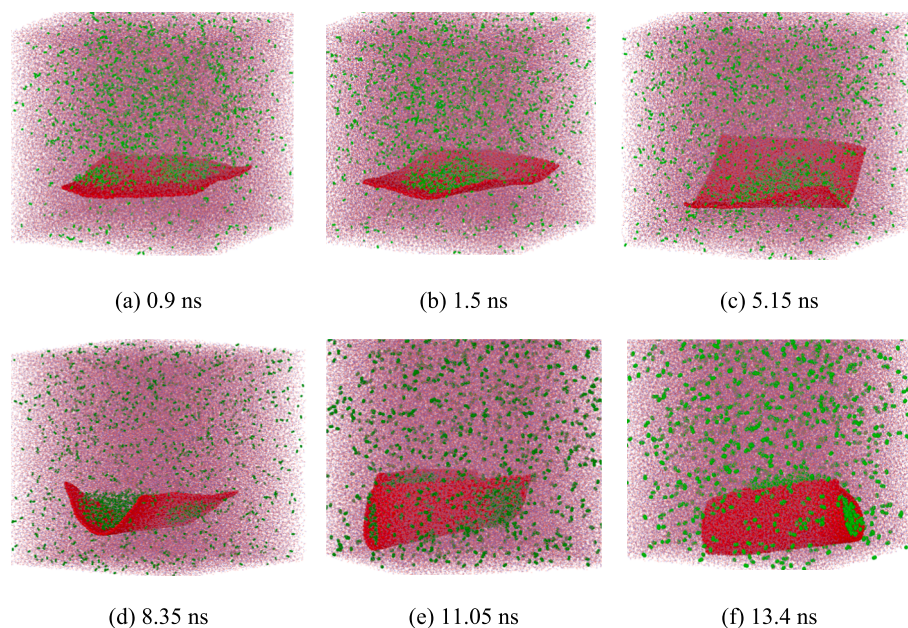


Fig. 1. Sequential snapshots illustrating the process of (a) initial site formation of oxygen (green) NBs on the G surface (red), (b) coalescence on the graphene surface, (c) movement of the formed NB to the edge of G, (d, e) adsorption of oxygen on the lower surface and migration to the unoccupied edge, and (f) encapsulation of the NB core by the G shell within the water NF.

of solid–liquid–gas interactions.

2. Theory and modelling

Computational nanotechnology emerges as a promising solution to tackle the challenges associated with studying NBs. These elusive entities present difficulties in terms of their capture and detection, often defying conventional predictions based on continuum theory. Remarkably, NBs exhibit prolonged stability that eludes full comprehension through the Epstein-Plesset theory at the nano-scale. Consequently, unraveling the behavior and characteristics of NBs becomes increasingly intricate, posing experimental limitations in laboratory investigations [20,38,39]. Leveraging computational approaches offers a valuable means to delve into the intricacies of NBs, shedding light on their properties and unveiling underlying mechanisms. Through the use of computational techniques, a broad range of NB characteristics and their effects can be explored. Quantum mechanics provides a means to understand the electronic structure of materials by solving the Schrödinger equation, but it is often time-consuming and restricted in sample types [40,41]. In contrast, molecular dynamics simulations offer a powerful tool to investigate complex systems from a molecular perspective, providing detailed insights into the structural and dynamic properties of substances in different states. By employing empirical potentials or force fields derived from quantum mechanics, alongside Newton's second law, molecular dynamics simulations accurately predict and track the interactions and movements of atoms under different conditions. The positions and velocities within molecular systems are influenced by the ensemble and chemical structure of the simulated system [42].

The interactions between solids, liquids, and gases play a significant role in numerous natural phenomena and industrial processes. Gaining a comprehensive understanding of how gases behave in liquids and their interactions at solid–liquid–gas interfaces is crucial for comprehending their behavior in engineered fluids and their thermophysical properties [43]. In this study, molecular dynamics simulations were employed to investigate the behavior and thermophysical properties of NFs. These NFs consisted of water and methanol and were prepared by dispersing G nanoparticles and dissolving gases such as N_2 , O_2 , H_2 , and CO_2 . The simulations were conducted at different temperatures and dissolved weight fractions. By utilizing molecular dynamics simulations, detailed

insights into the behavior and thermophysical properties of these hybrid NFs were obtained. The interactions among atoms in the system of methanol, water, gases, and G were simulated using a combination of force fields and potentials of all-atom optimized potentials for liquid simulations (OPLS), TIP4P/2005, Lenard-Jones, and Tersoff, respectively [44–51].

The simulations were performed using the open-source LAMMPS (Large-scale Atomic/Molecular Massively Parallel Simulator) software [52], and the Ovito software was utilized for visualization purposes [53]. The simulation systems comprised of boxes with dimensions of $15 \text{ nm} \times 15 \text{ nm} \times 15 \text{ nm}$, containing 98,000 water molecules and a G nanosheet composed of 3588 carbon atoms. Within these systems, a total of 2422 nitrogen molecules, 2120 oxygen molecules, and 1542 carbon dioxide molecules were scattered. Additionally, simulation boxes with the same G nanosheet and 48,000 methanol molecules were prepared, incorporating 2110 nitrogen molecules, 1850 oxygen molecules, and 1342 carbon dioxide molecules to achieve samples with same mass fractions. Moreover, 2422 and 2120 hydrogen molecules were distributed in the simulation boxes containing G water and G methanol, respectively. The prepared samples underwent relaxation and equilibration processes in different ensembles, including NPT for 1.7 ns and NVT for the same duration, to reach an equilibrium state at 298.15 K and 1 atm. Subsequently, the simulations were extended for an additional 10 ns in the NVE ensemble to study the behavior of G, NBs and the thermophysical properties of the G-based NFs, employing a time step of 1 fs. Additional information on the initial configurations and simulation procedure has been provided in the [supplementary file](#).

3. Results and discussion

3.1. Nanobubble nucleation and behaviour

In G-water NF containing oxygen, the initial stage involves the adsorption of oxygen molecules onto the G surface, leading to the formation of nucleation sites (Fig. 1a). Subsequently, these sites migrate and coalesce on the G surface, promoting the growth of NBs primarily at the edges of G, consequently inducing a gradual bending of the G structure (Fig. 1b and c). The absorption process persists as a result of the interactions between the absorbed molecules and the atoms on both

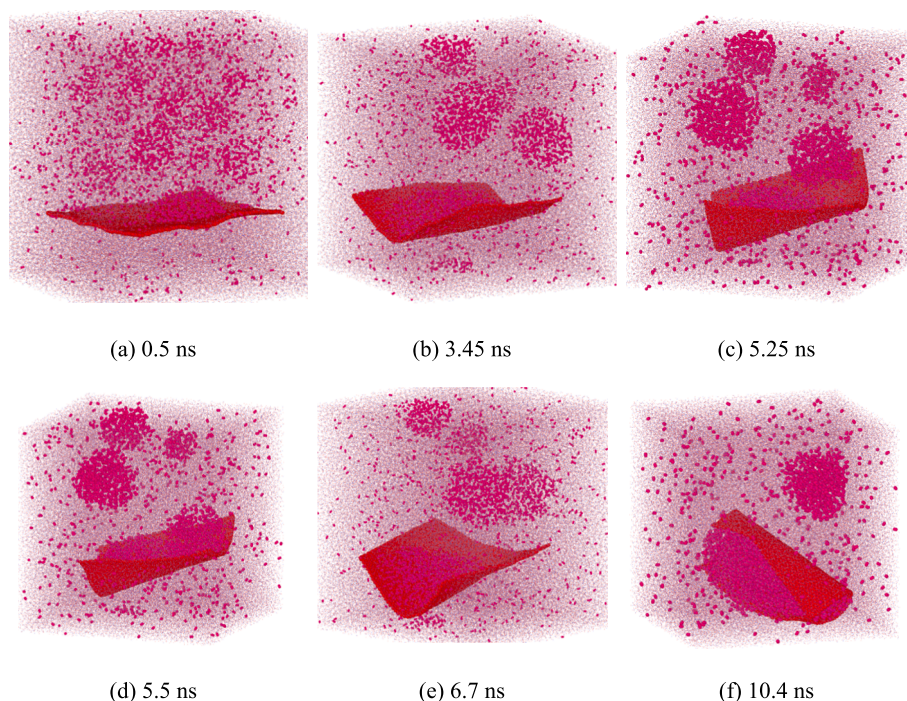


Fig. 2. Temporal snapshots illustrating the formation and behavior of nitrogen (pink) NBs in nitrogen/G-water NF over time.

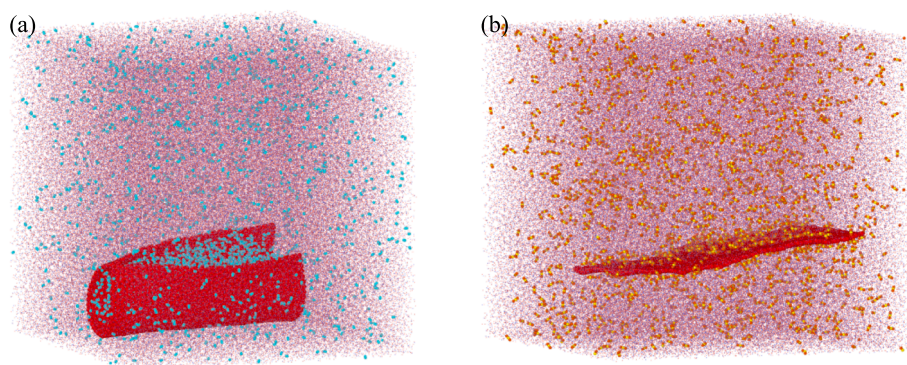


Fig. 3. Snapshot of the morphology of (a) hydrogen (cyan) and (b) carbon dioxide (brown) G-water NFs at 13.4 ns.

sides of the G, causing the adsorbed oxygen atoms on the lower surface to migrate towards an edge devoid of any adsorbed gas atoms (Fig. 1d and e). Eventually, the oxygen-covered edges merge together. The inherent tendency of oxygen atoms to diffuse into the formed NB, ultimately resulting in the formation of a NB core encapsulated by the G shell within the water-based NF (Fig. 1f).

In nitrogen-water NF, NB nucleation occurs on both G surface and in bulk fluid (Fig. 2a). Surface and bulk NBs merge, and nitrogen bulk NBs absorb into G from the unoccupied edge of G, converging with G surface NBs. This leads to a core-shell structure with a G shell encapsulating the NB core (Fig. 2b-e). The absorption process continues on the G surface, with gas atoms diffusing into the formed NB. Notably, nitrogen/

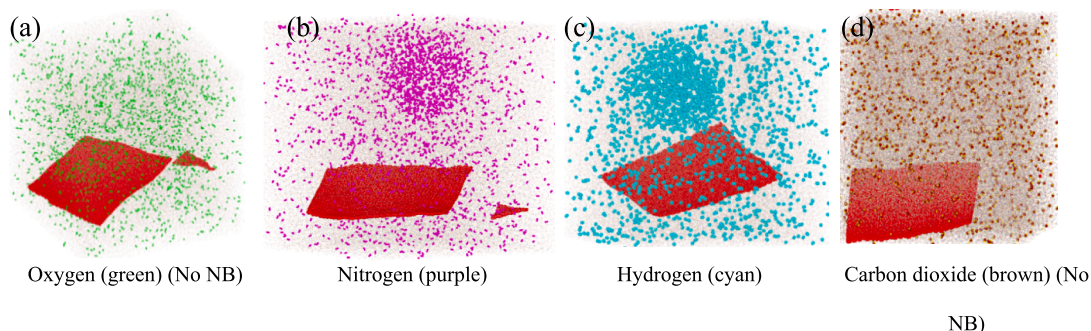


Fig. 4. At 13.4 ns, a visual representation captures the formation of NB in the G-methanol NF.

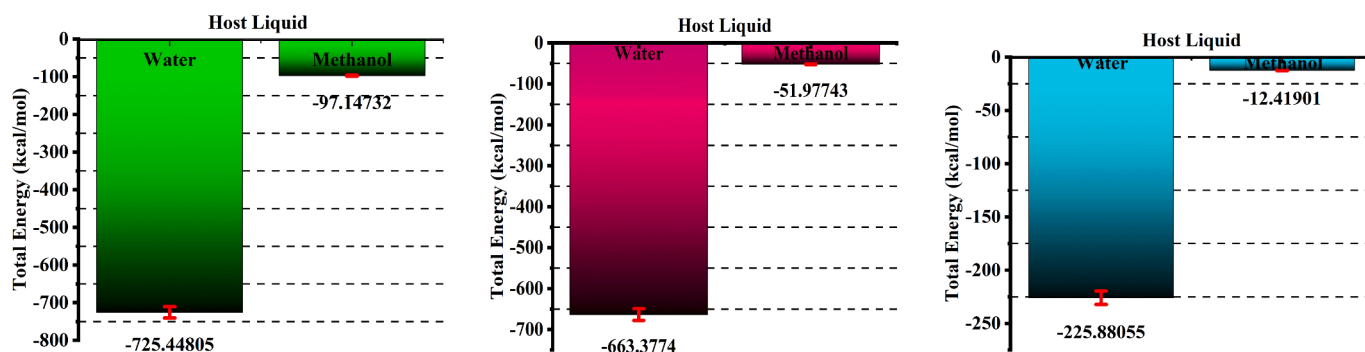


Fig. 5. The average of the total energy between oxygen (left), nitrogen (centre), and hydrogen (right) with G in water and methanol.

graphene-water NF contains both GNBs and bulk NBs (Fig. 2f).

The process of GNB formation in the hydrogen sample is similar to that in the oxygen sample, involving the creation of a GNB (Fig. 3a). However, the behavior of carbon dioxide is distinct, as no NBs were observed on the surface or within the bulk host fluid. The G sheet remained unbent, and only some carbon dioxide atoms were absorbed on the surface of G without NB formation (Fig. 3b).

To gain a deeper understanding of the observed intriguing behavior during the formation of graphene NBs in water-based NFs, comparative investigation was conducted using equivalent samples prepared in methanol as the host fluid under identical conditions. This comparative approach provides valuable insights into the underlying mechanisms behind these behaviors, facilitating a better understanding of the formation process in different fluid environments.

As depicted in Fig. 4 b and c, the behavior of nitrogen and hydrogen in methanol host fluids differs from that observed in water-based NFs. In

these cases, nitrogen and hydrogen molecules are not adsorbed onto the G surface, and the nucleation process occurs within the bulk of the host fluid. Furthermore, the formed nitrogen and hydrogen NBs within the host medium do not adsorb onto the graphene surface. An intriguing finding is related to the behavior of oxygen-G/methanol, where no surface or bulk NBs were observed, contrasting the observations in water-based samples (Fig. 4a). Similarly, the behavior of dissolved carbon dioxide in the G-methanol NF mimicked that of oxygen, with no surface or bulk NBs observed (Fig. 4d).

Graphene's unique electronic structure, determined by its arrangement of π orbitals, forms a bonding network across its hexagonal lattice of carbon atoms. These π bonds, originating from the overlap of carbon atom 2p orbitals, create a widespread electron system, enabling rapid movement and high mobility. When graphene wrinkles or crumples, the bonding environment of the carbon atoms shifts. This change leads to the formation of non-covalent bonds with graphene and nearby

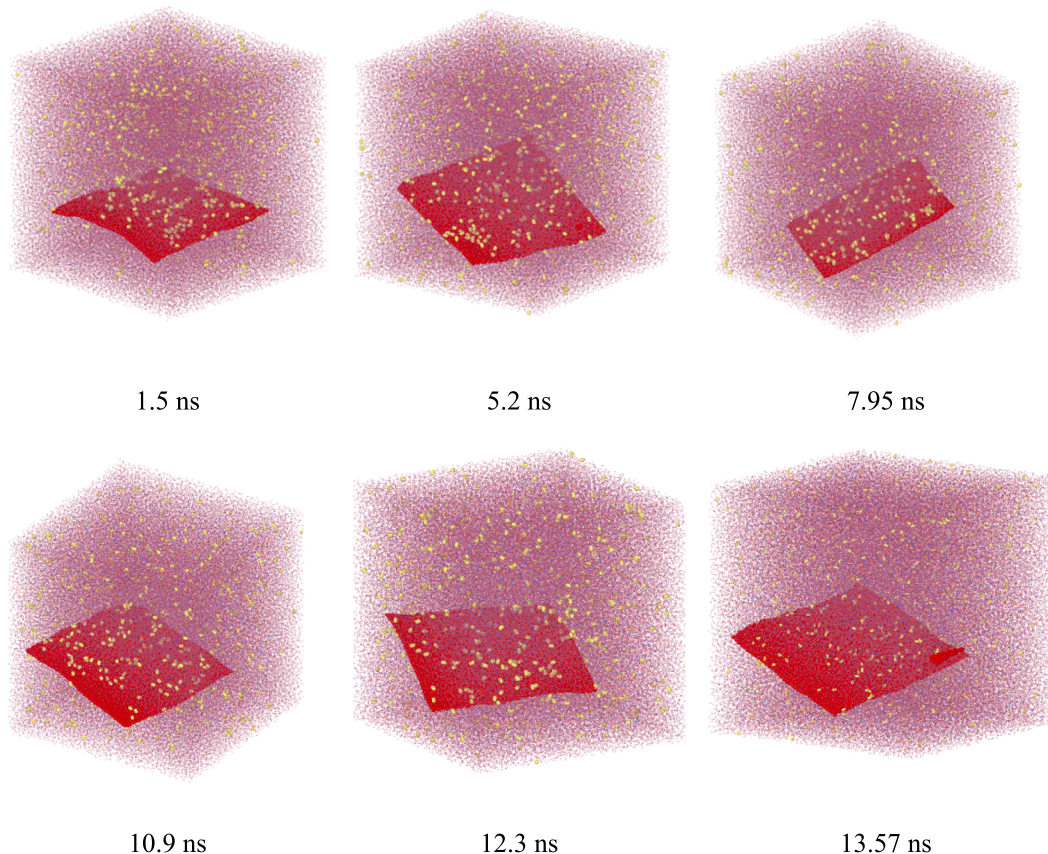


Fig. 6. Temporal evolution of nitrogen (yellow) cluster formation, movement, and disappearance with lower mass fractions of dissolved nitrogen gas within a G-water NF.

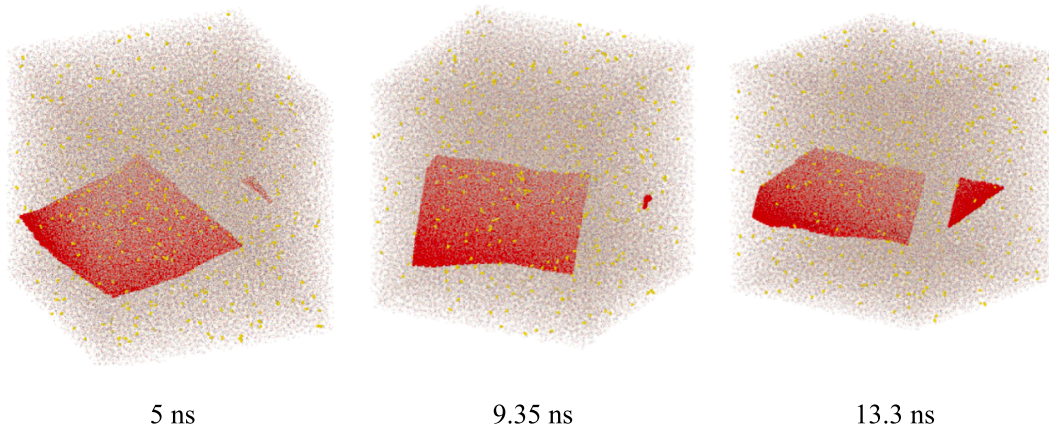


Fig. 7. Behaviour of dissolved nitrogen gas in G-methanol NF with lower mass fraction.

molecules, ions, or particles [54,55]. In water samples, the polar nature of water molecules, with a partial positive charge on hydrogen atoms and a partial negative charge on oxygen atoms, leads to strong hydrogen bonding between water molecules. This strong intermolecular force results in a high level of interaction among water molecules, leaving fewer interaction points available for other particles. On the other hand, the intermolecular forces in methanol are weaker compared to water, allowing for interactions with other molecules as well. When G and gases are dissolved in water, the strong interaction among water molecules limits their interaction with the host liquid. The π bond's tendency to seek attractive points for interaction results in a significant attractive force between gas molecules and G in water, leading to the absorption of gas molecules onto the G surface in water. However, in the case of methanol, the weaker interaction between the solvent molecules creates more available interaction points, reducing the attractive force between gas molecules and G in methanol. As a result, gas molecules do not absorb onto the G surface in methanol.

In Fig. 5, the average total energy associated with oxygen, nitrogen, and hydrogen's participation in GNB formation in water-based and methanol-hosted samples is depicted. The graph illustrates contrasting attractive forces in gas absorption behavior, providing insights into gas behavior and GNB formation. The interaction between dispersed graphene surfaces and dissolved gas is attributed to solvent molecule interactions, crucial in determining graphene structure and behavior. GNBs formed on graphene tend to migrate towards graphene edges, where carbon atoms have fewer neighboring atoms for bonding, leading to increased asymmetry and interaction sites. This localized asymmetry near edges exerts substantial force providing more interaction sites, resulting in the formed NBs preferentially occupying these particular regions.

To gain insights into the underlying mechanisms behind the observed behavior in G-NFs containing dissolved gases, particularly nitrogen, which exhibited intriguing behavior in both water and methanol-based fluids, a lower mass fraction of dissolved nitrogen, by scattering 605 molecules and 530 molecules in G-water and G-methanol NFs respectively, was investigated in graphene NFs. In the water-based sample, the lower mass fraction resulted in the absence of bulk nucleation, with only a small cluster of nitrogen gas atoms being absorbed onto the G surface. This surface cluster exhibited mobility but eventually dissipated, indicating the absence of NBs in both the surface and bulk forms (Fig. 6). Interestingly, in the methanol-based fluid, no nucleation occurred at all, emphasizing the influence of dissolved gas concentration on the nucleation process (Fig. 7).

The investigation of G behaviour in water-based fluids with various mass fraction of dissolved nitrogen gas revealed that, despite the formation of surface gas clusters at a lower mass fraction, no bending or deformation of the G surface was observed. Further analysis of the

nitrogen behavior on the G surface at higher mass fraction sample indicated that nitrogen gas atoms preferentially occupied the G edges, which have stronger interaction sites. The primary driving force behind the attractive interactions between nitrogen gas atoms was identified as the London dispersion forces. These forces arise from temporary distortions in the electronic distribution within the molecules, leading to transient dipole moments and subsequent attractive forces between neighboring molecules [56,57]. As a result, the nitrogen gas atoms were drawn together, akin to a bonding agent, causing them to approach and bond at the G edges (Fig. 2). This bonding mechanism contributed to the stability of the NBs formed on the G surface within the water-based NF. In essence, the presence of dissolved nitrogen and the interplay of London dispersion forces played a crucial role in maintaining the integrity of the G surface and supporting the formation of stable NBs.

3.2. Thermophysical properties

The thermophysical properties of NFs, specifically viscosity and heat capacity, play a significant role in their applications. To investigate these properties and understand the underlying mechanisms, a molecular-level approach was employed. In energy applications such as heat transfer systems and pumping processes, the viscosity of a fluid is of utmost importance. Higher viscosity can lead to increased frictional losses, diminishing overall energy transfer efficiency and requiring more energy for fluid pumping. Conversely, lower viscosity can enhance flow characteristics and reduce energy consumption. Therefore, gaining a comprehensive understanding of NF viscosity and developing methods to control it are vital for optimizing energy efficiency. The Green-Kubo method was utilized to calculate the viscosity of NFs, allowing for a detailed analysis of their flow characteristics and their potential impact on energy-related processes.

The Green-Kubo method was used to calculate the viscosity of the prepared samples, employing the following equation [58]:

$$\mu_{\alpha\beta}(t) = \frac{V}{k_B T} \int_0^t \langle P_{\alpha\beta}(0) P_{\alpha\beta}(t') \rangle dt' \quad (1)$$

where V represents the volume of the particle system, T denotes temperature, k_B is the Boltzmann constant, $\langle \dots \rangle$ signifies averaging over the ensemble employing the three distinct off-diagonal pressure tensor elements (P_{xy} , P_{yz} , P_{xz}) for $\alpha\beta \equiv x, y, z$, and t' and t represent time. The instantaneous value of the pressure tensor used in the Green-Kubo method is calculated at each time step, as described by the following equation [58]:

$$P_{\alpha\beta}(t) = \frac{\sum_{i=1}^K m_i u_{i\alpha}(t) u_{i\beta}(t)}{V} + \frac{\sum_{i=1}^K r_{i\alpha}(t) f_{i\beta}(t)}{V} \quad (2)$$

in which the pressure tensor value at time t , denoted as $P_{\alpha\beta}$, m_i

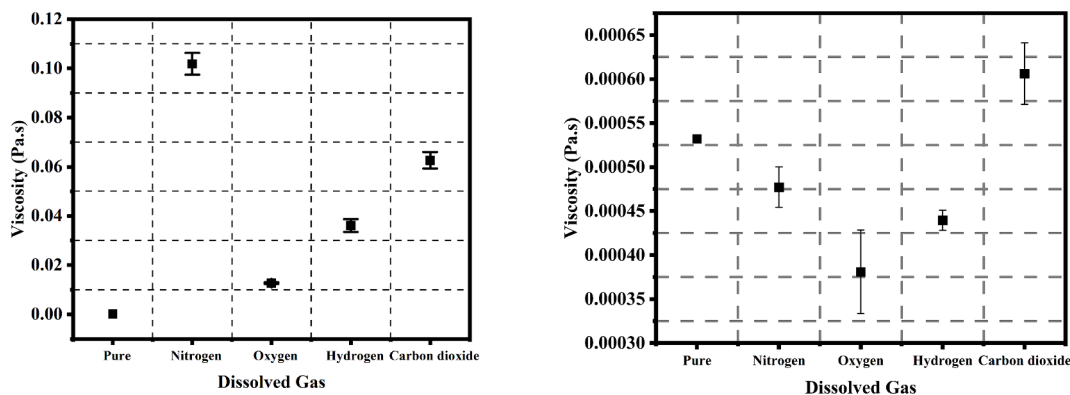


Fig. 8. Viscosity of G-water/scattered gas (left) and G-methanol/dissolved gas (right) NFs.

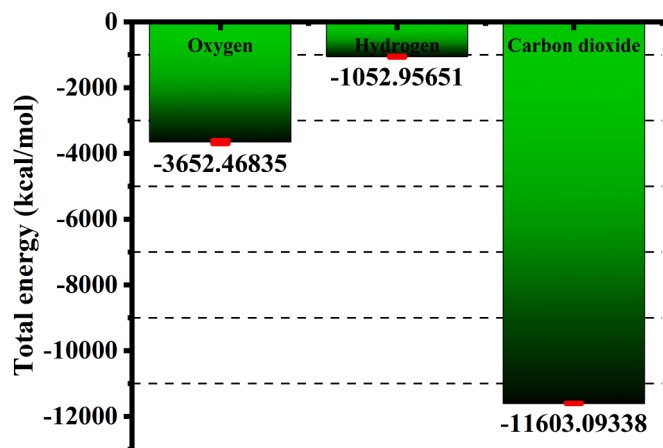


Fig. 9. The average of total energy between dissolved gases and water molecules.

represents the mass of atom i , $u_{i\alpha}$ and $u_{i\beta}$ are the velocities of atom i in the α and β directions, and $r_{i\alpha}$ and $f_{i\beta}$ are the position and force vector components of atom i . This calculation involves K atoms in the central simulation box. Additionally, when periodic boundary conditions are applied along with the minimum image convention, the sum is extended to encompass periodic image (ghost) atoms located outside of the central simulation box, denoted as K' .

Fig. 8 illustrates the viscosity of G-based NFs with dissolved gases in water and methanol. The results show that the inclusion of suspended G and dissolved gases, such as oxygen, nitrogen, carbon dioxide, and hydrogen, increases the viscosity of water NFs compared to the pure host liquids. Interestingly, in the case of methanol NFs, the dissolution of nitrogen, hydrogen, oxygen, and G results in a reduction in viscosity as opposed to pure methanol. Notably, the addition of carbon dioxide along with graphene to methanol causes an increase in viscosity. These findings are consistent with earlier research indicating that the viscosity of water tends to rise upon the incorporation of graphene [36] and gas dissolution [59]. However, there is a distinction between water and methanol. Unlike water fluid, it has been observed that the dissolution of gas in methanol actually leads to a decrease in viscosity [60]. Similar to the water, the presence of graphene increases the viscosity of methanol [37]. Consequently, it can be inferred that, for a given mass fraction of the prepared additive, the viscosity of methanol NFs is significantly influenced by the specific type of dissolved gas. In water-based nano-fluids incorporating graphene, the highest viscosity is achieved with nitrogen, followed by carbon dioxide, whereas the oxygen/G-water combination exhibits the lowest viscosity. In contrast, for methanol-based NFs containing G, the sample with carbon dioxide and G

exhibits the highest viscosity, while the presence of oxygen molecules results in the lowest viscosity.

The viscosity of NFs is influenced by hindered molecular motion and the interactions between suspended particles and the fluid. When NPs are present, they can impede the movement of molecules in the base fluid by acting as obstacles or impurities. This obstruction restricts the molecular motion, leading to an increase in viscosity. In the specific case of the nitrogen-G water system, as shown in Fig. 2, the existence of GNB, along with bulk NBs formed in the host liquids, formed bulk NB acts as obstacles against molecular motion, resulting in increased resistance to flow and a higher viscosity. The Green-Kubo equation, Eq. (1), involves the calculation of the instantaneous pressure tensor at each time step and as mentioned in Eq. 2, $f_{i\beta}$ is force vector components of atom i in the β directions. Moreover, force is the negative derivative of energy, and van der Waals energy signifies the attractive forces between atoms. When this energy is higher in one system compared to another, it implies that the attractive forces in the former system are stronger. Greater attractive forces restrict the movement of atoms, in turn, results in higher resistance to flow, ultimately leading to an increase in viscosity. By comparing the total energy between dissolved carbon dioxide, hydrogen, and oxygen molecules with water molecules in Fig. 9, it becomes evident that the strong force between carbon dioxide and water molecules limits the motion of the base fluid in the carbon dioxide sample. This stronger interaction between carbon dioxide and water hinders the molecular motion and increases the resistance to flow, resulting in a higher viscosity compared to the hydrogen and oxygen samples. Thus, the sample prepared with carbon dioxide exhibits a higher viscosity than the hydrogen and oxygen samples due to the specific nature of the interactions involved.

The joining of G edges is influenced by the London dispersion forces arising from the absorbed dissolved gases, as previously discussed. The strength of these forces depends on the polarizability of the involved molecules, with larger and more distant valence electrons exhibiting weaker electron-nucleus attractions and greater susceptibility to forming temporary dipoles. As a result, the London dispersion forces between oxygen molecules, being larger and more polarizable, are stronger compared to those between hydrogen molecules. Examining the morphology of suspended G in water with dissolved oxygen and hydrogen provides insights into the behavior of the absorbed molecules and their impact on the joining of G edges (Fig. 1). The higher London dispersion force associated with absorbed oxygen molecules facilitates

Table 1

The average total energy between dissolved gas and methanol molecules.

Dissolved gas	Total energy (Kcal/mol)
Oxygen	-4188.91
Carbon dioxide	-13158.47

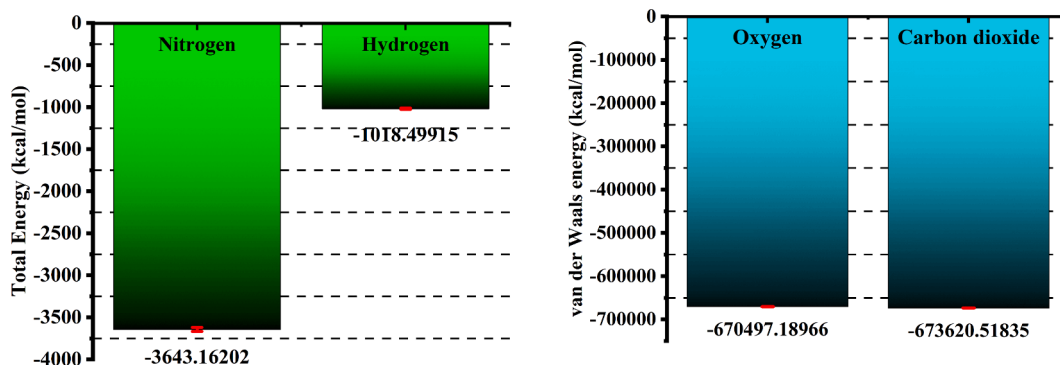


Fig. 10. The average total energy between dissolved gas and methanol molecules in bubbled (left) and the average van der Waals energy of non-bubbled methanol NFs.

Table 2

The viscosity (Pa.s) of G-water and G-methanol NFs with varying mass fractions of scattered nitrogen gas.

Host liquid	Lower mass fraction	Higher mass fraction
Water	0.10097	0.10183
Methanol	0.000637	0.000576

the complete joining of all G edges. In contrast, the lower London dispersion force of hydrogen allows only one edge of the G to join together (Fig. 3), while the other remains interactive with the surrounding environment. Consequently, in hydrogen-G/water sample, molecular interact with larger surface of G than the oxygen-G/water sample results in increased resistance to flow within the hydrogen-G/water NF, leading to a higher viscosity compared to the oxygen sample.

The viscosity of the carbon dioxide/G-methanol NF was found to be the highest, followed by the nitrogen/G-methanol NF, while the oxygen/G-methanol sample exhibited the lowest viscosity. To comprehend the influence of dissolved gas on the viscosity of methanol-based NFs, an analysis was conducted using non-bubbled methanol NFs with an identical mass fraction, incorporating only oxygen and carbon dioxide in methanol. This investigation revealed a reduction of 30.82 % and 2.44 % in the viscosity of methanol due to the dissolution of oxygen and carbon dioxide, respectively. The comparative total energy values between methanol molecules and the dissolved oxygen and carbon dioxide are presented in Table 1. Notably, the attractive forces between methanol molecules and carbon dioxide are found to be stronger than those between oxygen and methanol. This disparity in attractive forces contributes to the higher viscosity of methanol when carbon dioxide is present, as opposed to the case with oxygen. This underscores that the viscosity of the methanol sample is profoundly affected by the specific type of dissolved gas.

In the nitrogen and hydrogen/G-methanol sample, the presence of the NB acts as an obstacle, impeding the movement of molecules and resulting in augmented viscosity in G-methanol NFs containing nitrogen and hydrogen, in contrast to the sample with oxygen. In the hydrogen-G/methanol sample with NB, the attractive force between dissolved hydrogen and methanol atoms is weaker than nitrogen sample, resulting in a lower viscosity. Comparing the van der Waals energy of the non-bubbled carbon dioxide and oxygen samples reveals that the higher van der Waals energy in the carbon dioxide sample prevents molecules to move more freely compared to the oxygen sample (Fig. 10). These findings demonstrate that the viscosity of the samples is influenced by both the molecular interactions and the presence of NBs.

To delve deeper into the underlying mechanism of viscosity, the influence of lower mass fraction of dissolved nitrogen in G-based NFs was investigated, building upon the insights gained in the previous analysis. Table 2 presents the influence of mass fraction of dissolved nitrogen gas on the viscosity of G-based water and methanol-based NFs.

As indicated in Table 2, an augmentation in the mass fraction of dissolved gas yields a rise in the viscosity of water-based NFs and a decline in methanol-based NFs. This trend mirrors previous findings observed for both water [59] and methanol [61] NFs. Illustrated in Fig. 11 is the van der Waals energy of the water and methanol NFs, depicting that an upsurge in the mass fraction of dissolved nitrogen gas corresponds to an escalation in the van der Waals energy of water-based NF and a reduction in methanol-based NF. This increase in van der Waals energy engenders greater resistance to flow, consequently elevating the viscosity of water-based NF. Conversely, the decrease in van der Waals energy within methanol-based NF due to higher concentrations of dissolved gas facilitates freer molecular movement, resulting in a reduction in the viscosity of methanol NF.

Heat capacity is a fundamental property that quantifies the amount of heat energy a substance can absorb to raise its temperature by 1 °C. In

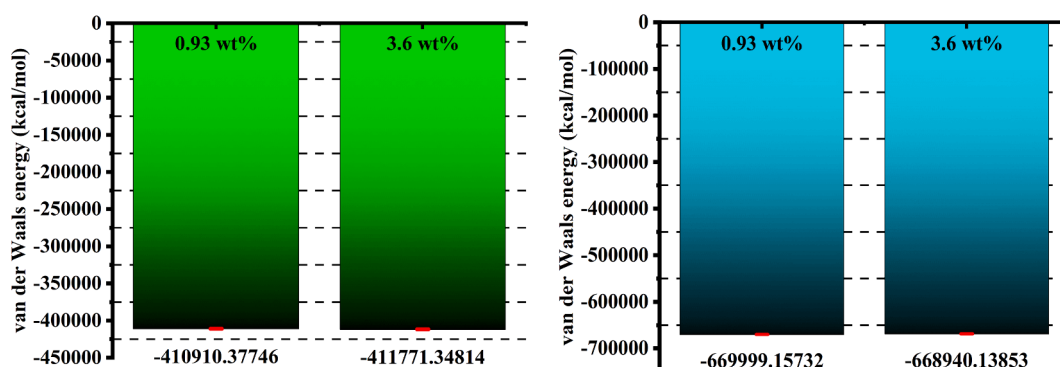


Fig. 11. The van der Waals energy of nitrogen/G-water NFs (left) and nitrogen/G-methanol NFs (right) at different mass fractions of scattered gas.

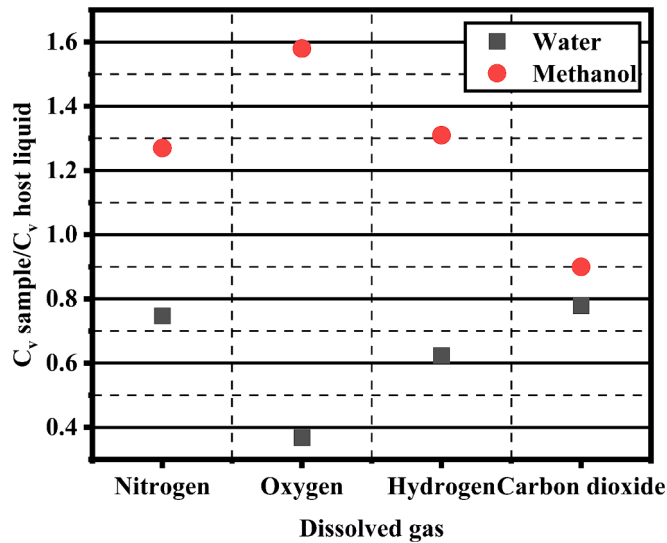


Fig. 12. Specific heat capacity of samples compared to the host mediums.

energy applications, efficient heat transfer is of paramount importance. One way to optimize the heat transfer performance of NFs is by modifying their heat capacity. By accurately calculating the heat capacity of NFs using appropriate equations and methodologies, it becomes possible to assess their ability to store and release thermal energy effectively. To quantify the heat storage capacity, the specific heat capacity at constant volume was computed using the following equation [62]:

$$C_v = \frac{\langle \delta E^2 \rangle}{K_B T^2} = \frac{\langle E^2 \rangle - \langle E \rangle^2}{K_B T^2} \quad (3)$$

where $\langle E^2 \rangle - \langle E \rangle^2$ is the fluctuation of energy, K_B is Boltzmann constant and T corresponds to the temperature. Fig. 12 illustrates the ratio of specific heat capacities between G-based NFs with dissolved gases in water and methanol to the specific heat capacities of their corresponding pure host liquids. The results highlight that incorporating G and dissolved gases in water-based NFs leads to a decrease in their specific heat capacity, corroborating prior studies [36].

Water exhibits a high heat capacity attributed to its distinctive molecular structure and the presence of hydrogen bonding, allowing it to absorb and retain a considerable amount of heat energy. However, with the introduction of G and gases to form water NFs, the overall heat capacity diminishes as graphene possesses a lower specific heat capacity compared to water. This decline can be attributed to the altered molecular interactions and the influence of G on the thermal properties of the NFs. Consequently, the specific heat capacity of the NFs is influenced by both the intrinsic properties of the host liquid and the presence of G and dissolved gases. The oxygen sample exhibited the largest reduction in heat capacity, while the carbon dioxide and nitrogen samples displayed comparatively smaller reductions compared to the oxygen-G/water NF. The Radial Distribution Function (RDF) provides valuable insights into the spatial distribution of particles and their probabilities at varying distances from a reference particle that can be calculated by using the following equation [63]:

$$x_i x_j \rho g_{ij}(r) = \frac{1}{N} \left\langle \sum_{i=1}^{N_i} \sum_{j=1}^{N_j} \delta(r + r_i - r_j) \right\rangle \quad (4)$$

in which x , ρ , $g(r)$, N , i , j , and ξ are mole fraction, density, RDF, the number of total atoms, and the types of chemicals, respectively.

Graphene can enhance heat transfer within the system, which directly influences the overall energy and heat capacity, Eq. (3). Increased impurities surrounding graphene lead to a decrease in energy distribution within the system. Fig. 13 visually represents the RDF

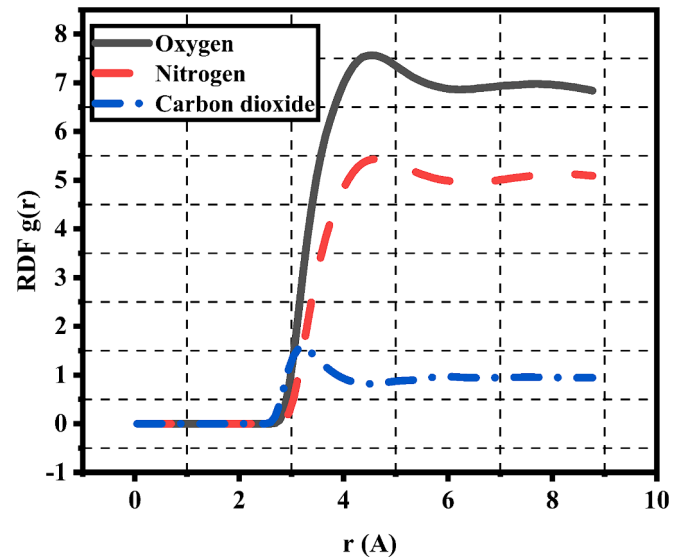


Fig. 13. The radial distribution function (RDF) of the same mass fraction dissolved gas in water samples with G nanosheet.

between the G nanosheet and dissolved gases, in NFs with the same mass fraction of dissolved gases, with the oxygen sample showing a higher peak, indicating a greater number of oxygen atoms surrounding the dispersed G in water. This disparity in peak heights suggests variations in the order structure of the systems, which can explain the observed differences in specific heat capacity among the samples. When oxygen is dissolved in water, it introduces additional complexity to the system by forming a gas-filled layer around G, which disrupts the heat transfer process and leads to a decrease in heat capacity. In the nitrogen NF, this layer exists to a lesser extent compared to the oxygen sample, resulting in a less pronounced effect on the heat capacity. As a result, the specific heat capacity of the nitrogen NF is higher than that of the oxygen NF. In the carbon dioxide sample, the G nanosheet remains relatively free from an extensive gas layer, allowing for a smoother and more efficient heat transfer process. This absence of a significant gas layer contributes to a higher heat capacity compared to the nitrogen sample. Therefore, the observed differences in heat capacity can be attributed to the variations in the order structure of the samples induced by the presence of dissolved gases surrounding the graphene nanosheet.

In contrast to water-based NFs, where the addition of G and dissolved gases decreases the specific heat capacity, the specific heat capacity of methanol host liquids increases with addition of nitrogen, oxygen, and hydrogen compared to pure methanol. This difference in heat capacity between water and methanol can be attributed to their distinct intermolecular interactions. The enhancement of heat capacity in NFs can be explained by three mechanisms [64]. Firstly, NPs have a higher heat capacity compared to their bulk counterparts due to the discretization of the phonon spectra and the modification of the phonon density of states. Secondly, the high surface area per unit mass of NPs induces an increase in the interfacial thermal resistance (ITR) between the NPs and the surrounding fluid molecules. This increase in ITR acts as additional thermal storage. Lastly, the presence of a solid-like layer formed by the nanolayering of liquid molecules around the NPs enhances the specific heat capacity due to the smaller intermolecular spacing compared to the bare fluid. As discussed earlier, methanol provides more interaction sites for the added nanomaterials, resulting in increased solid-liquid interactions. Furthermore, it has been demonstrated that NFs characterized by weak atomic bonding at the particle-fluid interface exhibit high thermal resistance, which could explain the enhanced specific heat capacity observed in the methanol-based fluid.

The introduction of oxygen gas into the G-methanol NF produced the most notable enhancement in specific heat capacity, followed by the

Table 3

The ratio of specific heat capacity between graphene-water and graphene-methanol nanofluids, relative to their respective pure fluids, for different weight fractions of dissolved gas.

Nanofluid based liquid	Lower weight fraction	Higher weight fraction
Water	1.09	0.747
Methanol	1.13	1.27

hydrogen addition. In the absence of NBs, the intermolecular forces between oxygen molecules and methanol were comparatively weaker when contrasted with the interactions between carbon dioxide and methanol, Table 1, possibly allowing greater mobility of oxygen molecules within the solution. This augmented molecular mobility could lead to heightened collision frequency and interactions between molecules. In the G-methanol sample containing NBs, hydrogen gas has a lower molecular weight, which promotes faster molecular motion. The enhanced molecular motion of hydrogen gas molecules allows them to effectively participate in heat transfer processes, contributing to the overall improvement in specific heat capacity. Moreover, the presence of NBs in the G-methanol NFs leads to higher specific heat capacity compared to non-bubbled carbon dioxide sample. NBs create additional interfaces between the gas phase and the liquid phase, increasing the interfacial thermal resistance. This results in a higher specific heat capacity in nano-bubbled G-methanol NFs. The hydrogen and nitrogen samples, where NBs were formed, exhibit a higher improvement in specific heat capacity than carbon dioxide sample due to the presence of these additional interfaces. However, it is worth noting that oxygen, despite not forming NBs, may still contribute to enhanced intermolecular interactions resulting in improvement in specific heat capacity. This underscores the significant influence of the specific dissolved gas on specific heat capacity, suggesting that intermolecular interactions play a more pivotal role in determining the specific heat capacity of NFs.

By examining the specific heat capacity of NFs at different mass fractions, a comprehensive understanding of the heat transfer behavior in these samples was obtained. Table 3 uncovers a fascinating relationship between the mass fraction of dissolved nitrogen in water-based and methanol-based GNFs and their specific heat capacity. Notably, the ratio of specific heat capacity exhibits distinct trends with increasing mass fraction, depending on the solvent. In water-based NFs, an increase in the mass fraction of dissolved gas leads to a decrease in specific heat capacity, while the opposite trend is observed in methanol-based NFs.

The remarkable thermal conductivity of G, owing to its unique lattice structure, facilitates enhanced heat transfer when introduced into a fluid. This augmentation in heat transfer efficiency enables the fluid to proficiently absorb and disseminate thermal energy, culminating in an elevation of heat capacity. Furthermore, the substantial surface area

relative to graphene's mass creates an abundance of intermolecular interaction sites within the fluid. These interactions bolster energy absorption and storage, thereby contributing to an elevated heat capacity. In water-based NFs, an intriguing observation arises while manipulating the mass fraction of dissolved gas. Elevated fractions of dissolved gas leads to the formation of additional gas layers around the graphene, as demonstrated by the RDF peak in Fig. 14. Additionally, the creation of graphene nanobubble in water-based NF, resulting from higher gas mass fractions, leads to the folding of G. This folding diminishes interaction sites, subsequently leading to reduced heat capacity. Conversely, in methanol-based NFs, an escalation in the dissolved gas mass fraction induces the formation of bulk NB. Notably, unlike water samples, this NB remains distanced from the G sheet in methanol. This spatial configuration diminishes the likelihood of gas atoms existing around the G in methanol-based NF, RDF peak in Fig. 14. The outcome is an increased heat capacity of G-methanol NFs as the dissolved gas mass fraction is augmented.

4. Conclusion

This study employs molecular dynamics simulations to explore the implications of solid-liquid-gas interactions on nanobubble formation within graphene-based water and methanol nanofluids, shedding light on their consequential effects on inherent nanofluid properties. The main conclusions can be drawn as follows:

- (1) The interaction between host liquids and dispersed gas species significantly influences nanobubble formation and graphene morphology in nanofluids. Strong water molecule interactions in polar-based nanofluids promote graphene nanobubble formation, facilitated by delocalized π electrons in graphene. Conversely, weaker interactions in methanol-based nanofluids lead to the absence of graphene nanobubbles, with only bulk nanobubbles present.
- (2) The introduction of additive particles in host liquids elevates water-based nanofluid viscosity, influenced by graphene nanobubble morphology. Additionally, the interaction between solvent molecules and dissolved gases affects viscosity. Specific heat capacity exhibits opposite trends between water and methanol-based nanofluids, attributed to molecular interactions and the presence of gas-filled nanolayers surrounding graphene.
- (3) In water-based NFs, increasing dissolved gas mass fosters the formation of graphene nanobubbles, causing graphene to fold and creating a gas layer around it, thereby reducing specific heat capacity. In methanol-based nanofluids, elevated dissolved gas mass induces the formation of bulk nanobubbles, diminishing gas

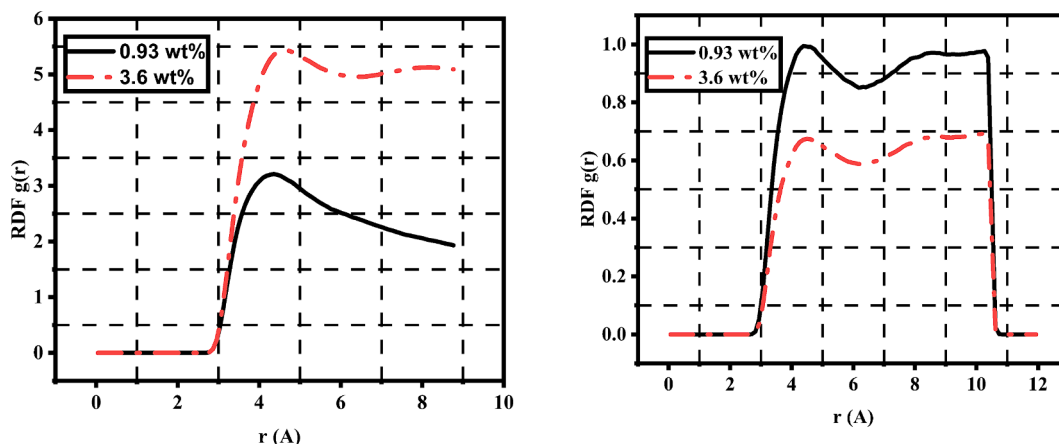


Fig. 14. The radial distribution function (RDF) of the different mass fraction of dissolved nitrogen gas in water (left) and methanol (right) NFs with G nanosheet.

atoms around graphene and increasing the heat capacity of graphene-methanol nanofluids.

CRedit authorship contribution statement

Hamidreza Hassanloo: Writing – review & editing, Writing – original draft, Methodology, Formal analysis, Data curation, Conceptualization. **Xinyan Wang:** Writing – review & editing, Supervision, Funding acquisition.

Declaration of competing interest

The authors declare that they have no known competing financial interests or personal relationships that could have appeared to influence the work reported in this paper.

Data availability

The data of this paper can be accessed from the Brunel University London data archive, figshare at <https://brunel.figshare.com>

Acknowledgement

This work was supported by a UKRI Future Leaders Fellowship (MR/T042915/1) and EPSRC DTP (EP/T518116/1-2688449). MD simulations were run on ARCHER2 and MMM Hub Young, the UK's National Supercomputing Service. The data of this paper can be accessed from the Brunel University London data archive, figshare at <https://brunel.figshare.com>.

Appendix A. Supplementary data

Supplementary data to this article can be found online at <https://doi.org/10.1016/j.fuel.2024.132517>.

References

- Hassan A, et al. Thermal management and uniform temperature regulation of photovoltaic modules using hybrid phase change materials-nanofluids system. *Renew Energy* 2020;145:282–93.
- Li X, Xie W, Sui C, Hsu P-C. Multispectral thermal management designs for net-zero energy buildings. *ACS Mater Lett* 2020;2(12):1624–43.
- Zhang Q, et al. Temperature-dependent dual-mode thermal management device with net zero energy for year-round energy saving. *Nat Commun* 2022;13(1):4874.
- Sathish T, et al. Effects of CuO/Al₂O₃/Water-WO₃ nanomaterials on NETZERO energy/emission-based hydrogen generation. *Fuel* 2023;343:127938.
- Mahian O, Kianifar A, Kalogirou SA, Pop I, Wongwises S. A review of the applications of nanofluids in solar energy. *Int J Heat Mass Transf* 2013;57(2):582–94.
- Sajid MU, Ali HM. Recent advances in application of nanofluids in heat transfer devices: a critical review. *Renew Sustain Energy Rev* 2019;103:556–92.
- Bakthavachalam B, Habib K, Saidur R, Saha BB, Irshad K. Comprehensive study on nanofluid and ionanofluid for heat transfer enhancement: A review on current and future perspective. *J Mol Liq* 2020;305:112787.
- Khanafer K, Vafai K. A review on the applications of nanofluids in solar energy field. *Renew Energy* 2018;123:398–406.
- Balandin AA, et al. Superior thermal conductivity of single-layer graphene. *Nano Lett* 2008;8(3):902–7.
- Lee C, Wei X, Kysar JW, Hone J. Measurement of the elastic properties and intrinsic strength of monolayer graphene. *Science* 2008;321(5887):385–8.
- Bolotin KI, et al. Ultrahigh electron mobility in suspended graphene. *Solid State Commun* 2008;146(9–10):351–5.
- Stoller MD, Park S, Zhu Y, An J, Ruoff RS. Graphene-based ultracapacitors. *Nano Lett* 2008;8(10):3498–502.
- Gadipelli S, Guo ZX. Graphene-based materials: synthesis and gas sorption storage and separation. *Prog Mater Sci* 2015;69:1–60.
- Kanti P, Minea AA, Sharma K, Revanasiddappa M. Improved thermophysical properties of Graphene Ionanofluid as heat transfer fluids for thermal applications. *J Ionic Liquids* 2022;2(2):100038.
- Yavari F, Koratkar N. Graphene-based chemical sensors. *J Phys Chem Lett* 2012;3(13):1746–53.
- Shao Y, Wang J, Wu H, Liu J, Aksay IA, Lin Y. Graphene based electrochemical sensors and biosensors: a review. *Electroanalysis: Int J devoted to Fundamental Practical Aspects Electroanalysis* 2010;22(10):1027–36.
- Graziano G. Forever blowing nanobubbles. *Nat Rev Chem* 2020;4(10).
- An H, Tan BH, Moo JGS, Liu S, Pumera M, Ohl C-D. Graphene nanobubbles produced by water splitting. *Nano Lett* 2017;17(5):2833–8.
- Hu H, et al. Quasi/non-equilibrium state in nanobubble growth trajectory revealed by in-situ transmission electron microscopy. *Nano Today* 2023;48:101761.
- Alheshibri M, Qian J, Jehannin M, Craig VS. A history of nanobubbles. *Langmuir* 2016;32(43):11086–100.
- Zamborlini G, et al. Nanobubbles at GPa pressure under graphene. *Nano Lett* 2015;15(9):6162–9.
- Ohgaki K, Khanh NQ, Joden Y, Tsuji A, Nakagawa T. Physicochemical approach to nanobubble solutions. *Chem Eng Sci* 2010;65(3):1296–300.
- Zhou L, Wang S, Zhang L, Hu J. Generation and stability of bulk nanobubbles: a review and perspective. *Curr Opin Colloid Interface Sci* 2021;53:101439.
- Alheshibri M, Craig VS. Generation of nanoparticles upon mixing ethanol and water; Nanobubbles or Not? *J Colloid Interface Sci* 2019;542:136–43.
- Weijs JH, Seddon JR, Lohse D. Diffusive shielding stabilizes bulk nanobubble clusters. *ChemPhysChem* 2012;13(8):2197–204.
- Gao Z, Wu W, Sun W, Wang B. Understanding the stabilization of a bulk nanobubble: a molecular dynamics analysis. *Langmuir* 2021;37(38):11281–91.
- Li C, Zhang A, Wang S, Cui P. Formation and coalescence of nanobubbles under controlled gas concentration and species. *AIP Advances*, 2018; 8(1).
- Iakovlev E, Zhilyaev P, Akhatov I. Atomistic study of the solid state inside graphene nanobubbles. *Sci Rep* 2017;7(1):17906.
- Dockar D, Borg MK, Reese JM. Mechanical stability of surface nanobubbles. *Langmuir* 2018;35(29):9325–33.
- Mi F, He Z, Jiang G, Ning F. Effects of marine environments on methane hydrate formation in clay nanopores: a molecular dynamics study. *Sci Total Environ* 2022;852:158454.
- Hong S-N, Ri J-H, Mun S-Y, Yu C-J. Revealing the influence of porosity and temperature on transport properties of nanobubble solution with molecular dynamics simulations. *J Mol Liq* 2022;367:120518.
- Qu Z-X, Wang B-S, Jiang J-W. The gas in graphene bubbles: an improved van der Waals equation description. *J Phys Chem C* 2023;127(19):9205–12.
- Bird E, Smith E, Liang Z. Coalescence characteristics of bulk nanobubbles in water: a molecular dynamics study coupled with theoretical analysis. *Phys Rev Fluids* 2021;6(9):093604.
- Heyhat MM, Rajabpour A, Abbasi M, Arabha S. Importance of nanolayer formation in nanofluid properties: Equilibrium molecular dynamic simulations for Ag-water nanofluid. *J Mol Liq* 2018;264:699–705.
- Ahmed N, Asirvatham LG, Wongwises S. Effect of volume concentration and temperature on viscosity and surface tension of graphene–water nanofluid for heat transfer applications. *J Therm Anal Calorim* 2016;123:1399–409.
- Elsaid K, et al. Thermophysical properties of graphene-based nanofluids. *Int J Thermofluids* 2021;10:100073.
- Sarafraz M, Safaei MR. Diurnal thermal evaluation of an evacuated tube solar collector (ETSC) charged with graphene nanoplatelets-methanol nano-suspension. *Renew Energy* 2019;142:364–72.
- Häbich A, Ducker W, Dunstan DE, Zhang X. Do stable nanobubbles exist in mixtures of organic solvents and water? *J Phys Chem B* 2010;114(20):6962–7.
- Epstein PS, Plesset MS. On the stability of gas bubbles in liquid-gas solutions. *J Chem Phys* 1950;18(11):1505–9.
- Bader R. Quantum topology of molecular charge distributions. III. The mechanics of an atom in a molecule. *J Chem Phys* 1980;73(6):2871–83.
- Tanner DJ, et al. Accurate first principles calculation of molecular charge distributions and solvation energies from ab initio quantum mechanics and continuum dielectric theory. *J Am Chem Soc* 1994;116(26):11875–82.
- Allen MP. Introduction to molecular dynamics simulation. *Computational Soft Matter: Synthetic Polymers Proteins* 2004;23(1):1–28.
- Wang W, et al. Solid–liquid–gas reaction accelerated by gas molecule tunnelling-like effect. *Nat Mater* 2022;21(8):859–63.
- Jorgensen WL, Maxwell DS, Tirado-Rives J. Development and testing of the OPLS all-atom force field on conformational energetics and properties of organic liquids. *J Am Chem Soc* 1996;118(45):11225–36.
- Zaragoza A, et al. Molecular dynamics study of nanoconfined TIP4P/2005 water: how confinement and temperature affect diffusion and viscosity. *PCCP* 2019;21(25):13653–67.
- Jain S, Qiao L. Molecular dynamics simulations of the surface tension of oxygen-supersaturated water. *AIP Adv* 2017;7(4).
- Chae K, Violi A. Mutual diffusion coefficients of heptane isomers in nitrogen: a molecular dynamics study. *J Chem Phys* 2011;134(4):pp.
- Yang Q, Zhong C. Molecular simulation of adsorption and diffusion of hydrogen in metal–organic frameworks. *J Phys Chem B* 2005;109(24):11862–4.
- Sun C, Wen B, Bai B. Application of nanoporous graphene membranes in natural gas processing: Molecular simulations of CH₄/CO₂, CH₄/H₂S and CH₄/N₂ separation. *Chem Eng Sci* 2015;138:616–21.
- Tersoff J. Modeling solid-state chemistry: Interatomic potentials for multicomponent systems. *Phys Rev B* 1989;39(8):5566.
- Grossman J, Ferralis N, Cohen-Tanugi D, Dave SH. Porous materials and methods including nanoporous materials for water filtration. *Google Patents*, 2014.
- Plimpton S. Fast parallel algorithms for short-range molecular dynamics. *J Comput Phys* 1995;117(1):1–19.
- Stukowski A. Visualization and analysis of atomistic simulation data with OVITO—the Open Visualization Tool. *Model Simul Mater Sci Eng* 2009;18(1):015012.
- Zhan J, Lei Z, Zhang Y. Non-covalent interactions of graphene surface: mechanisms and applications. *Chem* 2022.

- [55] Deng S, Berry V. Wrinkled, rippled and crumpled graphene: an overview of formation mechanism electronic properties and applications. *Mater Today* 2016;19(4):197–212.
- [56] Alavi S. *Molecular simulations: fundamentals and practice*. John Wiley & Sons; 2020.
- [57] Dill K, Bromberg S. *Molecular driving forces: statistical thermodynamics in biology chemistry physics and nanoscience*. Garland Science; 2010.
- [58] Mathas D, et al. Evaluation of methods for viscosity simulations of lubricants at different temperatures and pressures: a case study on PAO-2. *Tribol Trans* 2021;64(6):1138–48.
- [59] Kumagai A, Kawase Y, Yokoyama C. Falling capillary tube viscometer suitable for liquids at high pressure. *Rev Sci Instrum* 1998;69(3):1441–5.
- [60] Kerscher M, et al. Thermophysical properties of the energy carrier methanol under the influence of dissolved hydrogen. *Int J Hydrogen Energy* 2023.
- [61] Turner C. From supercritical carbon dioxide to gas expanded liquids in extraction and chromatography of lipids. *Lipid Technol* 2015;27(12):275–7.
- [62] Engelmann S, Hentschke R. Specific heat capacity enhancement studied in silica doped potassium nitrate via molecular dynamics simulation. *Sci Rep* 2019;9(1):7606.
- [63] Hansen J-P, McDonald IR. *Theory of simple liquids: with applications to soft matter*. Academic press; 2013.
- [64] Rodríguez-Laguna M d R, et al. Mechanisms behind the enhancement of thermal properties of graphene nanofluids. *Nanoscale* 2018;10(32):15402–9.